MATERIALS CHEMISTRY
FRONTIERS

RESEARCH ARTICLE

View Article Online
View Journal | View Issue

Cite this: *Mater. Chem. Front.*, 2024, **8**, 3949

Fine-tuning of core–shell 1D nanoparticles for thermally conductive, yet electrically insulating, 3D-printable polymer nanocomposites†

Antoine Bodin, Thomas Pietri, Caroline Celle and Jean-Pierre Simonato *

Core–shell nanostructures are particularly interesting for the development of dual-property nanofillers for nanocomposites. In this study, advanced materials compatible with the commonly used fused deposition modeling (FDM) 3D printing technique are reported for heat dissipation applications. Core–shell nanowires based on a highly thermally conductive silver core coated with an electrically insulating silica shell are investigated. The heat dissipation performance of polycarbonate nanocomposites is analyzed using a comprehensive set of thermal, electrical, mechanical, and rheological characterization studies to determine the optimal silica nanolayer thickness. We demonstrate that these core–shell nanofillers give access to both high thermal conductivity of up to 2.08 ± 0.05 W m^{-1} K^{-1}, and electrically insulating behavior (electrical resistivity $>10^{12}$ Ω cm) at only 3 vol% loading, while retaining very good mechanical strength. The high dispersion and interfacial cohesion of the nanomaterials with the matrix play a key role in achieving these performances. Moreover, thanks to the alignment of the 1D nanofillers during the FDM printing process, the thermal conductivity of the PC nanocomposite reaches an unprecedented value of 3.48 ± 0.06 W m^{-1} K^{-1} in the printing direction, *i.e.* a fifteen-fold increase over the thermal conductivity of neat PC.

Received 17th June 2024,
Accepted 2nd October 2024

DOI: 10.1039/d4qm00520a

rsc.li/frontiers-materials

Introduction

The rapid growth of microelectronics and energy storage technologies is giving rise to increasingly powerful systems that simultaneously require greater miniaturization and further integration of components, thereby generating undesirable and potentially damaging heat for systems in operation.[1,2] Indeed, novel fast-charging batteries with high energy densities trigger high heat generation rates during charging and discharging cycles. This heat accumulation can lead to thermal runaways threatening the integrity of batteries, raising safety issues.[3–5] Similarly, the development of increasingly powerful microprocessors in ever-shrinking dedicated volumes leads to the build-up of hotspots since high integration of transistors has resulted in the escalation of power dissipation and heat generation in microelectronic devices. If heat is not properly dissipated, overheating of the electronic components will inevitably have a detrimental influence on their lifespan and reliability.[6,7] The lack of space for convection cooling systems in portable devices entails the need for developing a new class of heat dissipative structural materials. Henceforth, improving the performance of batteries and electronic systems now heavily depends on the efficiency of their thermal management. In addition to the good thermal conductivity required to facilitate heat dissipation, these new materials also need to provide good electrical insulation to avoid electrical issues such as short-circuits, power overconsumption or signal propagation delay.[7–9]

Thermoplastic polymer materials offer great potential to meet these needs, thanks to their intrinsic electrical insulation, low cost and ease of processing. However, pure polymeric materials generally exhibit very limited thermal conductivity (<0.3 W m^{-1} K^{-1}).[10] A promising strategy for improving thermal conductivity while preserving electrical insulation of polymer-based materials is to incorporate thermally conductive yet electrically insulating fillers into the polymer matrix. Several types of thermally conductive fillers have been studied over the past few years including particles made of carbon,[11–14] metals,[15,16] and ceramics.[17–19] Carbon-based and metallic fillers generally show very high intrinsic thermal conductivity. However, they also exhibit high electrical conductivity.[14,20–22] Ceramics lack free electrons, they are therefore inherently electrically insulating, but as a corollary less thermally conductive.[10,23] In order to take advantage of the high thermal conductivity of electrically conductive fillers, core@shell

Univ. Grenoble Alpes, CEA, LITEN, F-38000 Grenoble, France.
E-mail: jean-pierre.simonato@cea.fr

† Electronic supplementary information (ESI) available. See DOI: https://doi.org/10.1039/d4qm00520a

nanostructures combining a highly thermally conductive core and an electrically insulating shell have been investigated.[24–28] In order to prevent electrical conduction throughout the composite, the shell must efficiently hinder the transport of electrical charges between nanofillers. Shells made of ceramic material such as silica (SiO_2) appear to be ideal candidates for meeting this requirement.[29–33] Compared with larger particles, nanofillers are able to build many more thermally conductive paths through the composite, which is beneficial for thermal dissipation purposes.[34] Although much less studied than 0D nanoparticles, 1D nanofillers with high aspect ratios are preferable as they ensure improved thermal conductivity through the formation of a 3D percolating network at lower loading ratios, thereby avoiding high viscosities and processability issues.[35–37] This is particularly important in our study since we aim at developing nanocomposites printable by the FDM 3D printing technology, which adds an extra level of difficulty regarding the necessary achievement of complementary properties to reach good printability (*e.g.* adequate rheology, thermal stability, *etc.*).[38] The possibility of using 3D printing is a major expected outcome of this study, the aim being to produce complex shapes designed on demand to optimize the thermal dissipation of various devices.[39]

In the present study, we report on the use of silver nanowires (AgNWs) as the core material for core@shell nanostructures, as silver is the metal displaying the highest thermal conductivity, and because some silver-based core–shell derivatives have already displayed interesting performances for non-printable nanocomposites.[32,40,41] On another note, AgNW@SiO_2 core–shell nanostructures have also been used recently in other fields of research, showing that they might be of interest in a wide range of applications.[42,43] We demonstrate how a fine tuning of conformal silica nanolayers on the surface of AgNWs induces major changes in the performances of polycarbonate (PC) nanocomposites. The effect of the silica interface with the PC matrix and the influence of its thickness on thermal, electrical, rheological and mechanical properties of the nanocomposites are presented. In addition, the influence of the 3D printing process on the orientation and alignment of the 1D nanostructures was investigated and the resulting variations in thermal conductivity are discussed.

Results and discussion

AgNW@SiO_2 core–shell nanofillers

The thickness of the SiO_2 layer on AgNWs was controlled through a fine adjustment of the TEOS content during the synthesis (Fig. 1(a)). TEOS amounts of 0.325%, 0.65%, 1.30%, 2.00% and 4.00% respectively yielded SiO_2 thicknesses of 5, 11, 20, 27 and 43 nm on the surface of AgNWs, leading to AgNW@SiO_2 core–shell samples referred hereinafter as AgNW@SiO_2-5, AgNW@SiO_2-11, AgNW@SiO_2-20, AgNW@SiO_2-27 and AgNW@SiO_2-43 respectively. FE-SEM images of pure and silica coated AgNWs are displayed in Fig. 1(b)–(h).

Applying an accelerating voltage of 10 kV revealed the SiO_2 shell through contrast improvement between the heavy Ag core and the lighter SiO_2 shell. This is highlighted in Fig. 1(b)–(g) insets and in the high-resolution images of lateral views of each synthesized AgNW@SiO_2 core–shell nanostructure presented in Fig. 1(h). All samples were coated by a smooth and conformal SiO_2 layer, except for AgNW@SiO_2-5 (Fig. 1(c)) which displayed a layer mainly made of agglomerated and unmerged SiO_2 nanoparticles, and AgNW@SiO_2-11 (Fig. 1(d)) which exhibited a slightly rougher SiO_2 layer compared to other samples. The EDX analysis performed on AgNWs treated with TEOS (Fig. 1(i)) revealed the Ag core as well as both Si and O emission lines (Fig. S2, ESI†), confirming the existence of a continuous SiO_2 shell at the surface of AgNW@SiO_2-20, AgNW@SiO_2-27 and AgNW@SiO_2-43. A set of complementary analyses using FTIR spectroscopy and XPS was carried out to confirm unambiguously the chemical composition and the core–shell structure of the nanomaterials (Fig. S3 and S4, ESI†). Contrary to what had been observed with pure AgNWs that irreversibly agglomerate once filtered, all AgNW@SiO_2 samples were easily redispersed in ethanol or chloroform after vacuum filtration (Fig. S5, ESI†), proving that the SiO_2 shell improves dramatically the dispersion of the AgNWs.

The condensation of TEOS on the AgNWs was made possible, thanks to a thin residual layer of polyvinylpyrrolidone (PVP) adsorbed on the metallic surface after the synthesis of AgNWs (highlighted by the carbon emission line spotted in EDX mappings presented in Fig. S2, ESI†). Indeed, the polyol synthesis of AgNWs requires the use of PVP which acts notably as a very thin encapsulating layer.[44,45] During the shell fabrication, PVP functional groups assist the SiO_2 layer synthesis, acting as preferential condensation sites for grafting hydrolyzed TEOS molecules onto the PVP enolized form.[46] The SiO_2 nanolayer formation can be described by a nucleation/growth mechanism as depicted in Fig. S6 (ESI†). At the very beginning of the SiO_2 nanolayer synthesis, hydrolyzed TEOS molecules ($Si(OEt)_{4-n}(OH)_n$ with $1 \leq n \leq 4$) start to condense on the AgNW surface through a heterogeneous nucleation mechanism. Following this preliminary nucleation step, the more hydrolyzed molecules reach the nanowire surface, the more the reaction shifts towards a condensation and coalescence mechanism until a continuous SiO_2 nanolayer is formed. The initial concentration of TEOS for the formation of a conformal and continuous SiO_2 nanolayer lies between 0.65 and 1.30% v/v to ethanol (corresponding to AgNW@SiO_2-11 and AgNW@SiO_2-20 respectively). During the formation of the silica layer, pure silica particles can form. In order to purify the core–shell nanowires, the solution is vacuum filtered several times over a 1.2 μm PTFE membrane to get rid of free silica nanoparticles. Once purified, the AgNW@SiO_2 core–shell nanostructures with various SiO_2 shell thicknesses were dispersed in the PC matrix to produce PC-AgNW@SiO_2 nanocomposites.

Morphology of PC-AgNWs and PC-AgNW@SiO_2 nanocomposites

Pure AgNWs and the five AgNW@SiO_2 samples were infused within the PC matrix to investigate the influence of the SiO_2 shell thickness on the physical properties of the nanocomposites.

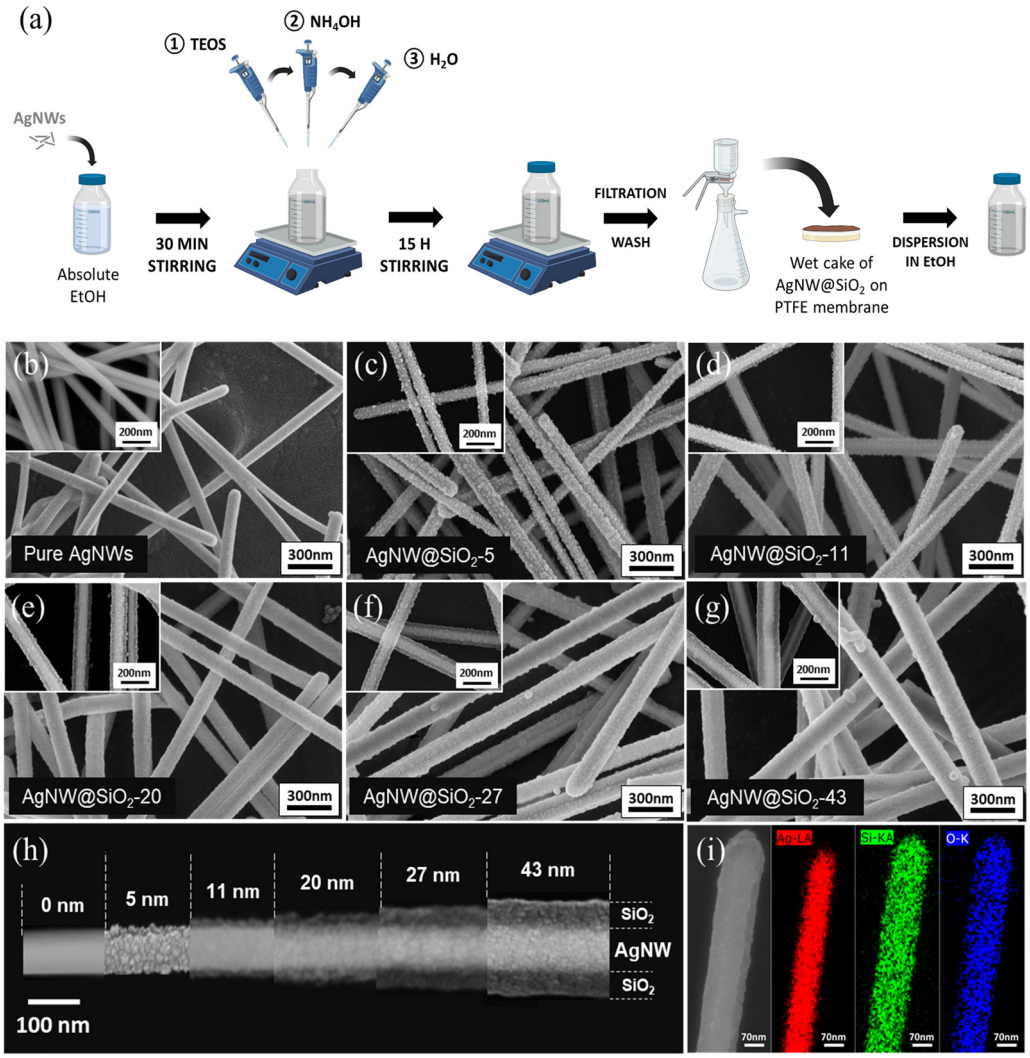

Fig. 1 (a) Synthesis process of AgNW@SiO_2 nanostructures; FE-SEM images of (b) pure AgNWs and (c)–(g) AgNW@SiO_2 core–shell nanowires with thicknesses varying from 5 to 43 nm (5 kV accelerating voltage). Insets are images taken at 10 kV accelerating voltage; (h) photomontage of an AgNW core coated with a SiO_2 shell of increasing thicknesses (10 kV accelerating voltage); (i) EDX mapping of a single AgNW@SiO_2-27 nanowire.

PC was chosen because of its very interesting mechanical properties as well as its superior dimensional and thermal stabilities. Moreover, PC is a high-performance, heat-resistant thermoplastic polymer that can be easily processed by FDM 3D printing.[47] Before studying the PC-AgNW@SiO_2 nanocomposite, loadings of 0.5, 1, 3, 5 and 7 vol% were studied for the PC-AgNW reference composite, which permitted to choose the most suitable loading ratio (3 vol%) for the following PC-AgNW@SiO_2 study (see the ESI† for details).

Fractured surfaces of PC-AgNWs and PC-AgNW@SiO_2-5 to PC-AgNW@SiO_2-43 samples loaded with 3 vol% of nanofillers were observed by FE-SEM to appraise the dispersion of the nanofillers and their interfacial compatibility with the PC matrix (Fig. 2(b)–(d)). The micrograph of the PC-AgNW sample (Fig. 2(b)) clearly shows a separation between the PC matrix and the AgNWs which are mainly agglomerated. Moreover, it was observed that pure AgNWs do not exhibit high compatibility with the PC matrix (Fig. 2(c)). The repulsive effect encountered between the nanofillers and the polymer matrix leads to low adhesion and creates voids between AgNWs and PC, which results in an increase of the interfacial thermal contact resistance. In contrast, the samples with AgNW@SiO_2 nanofillers display a much better filler–matrix interaction as individual core–shell nanowires are fully embedded and well distributed within the nanocomposites (Fig. 2(d) and (e)). This behavior has already been reported for epoxy nanocomposites, where the SiO_2 nanolayer coated on the AgNWs were shown to enhance the wetting of epoxy on the AgNW@SiO_2 surfaces, due to the presence of hydroxyl groups on the silica surface.[32] The AgNW@SiO_2 nanofillers were homogeneously and highly dispersed in the PC matrix as a result of a better interfacial cohesion, directly through the solution mixing process. No significant difference was observed on fractured surfaces between the various PC-AgNW@SiO_2 nanocomposites (Fig. S8, ESI†). As expected, these images of nanocomposite fractured surfaces show that nanofillers are oriented in a specific plane, in a direction perpendicular to the hot-pressing axis. Additionally, adding

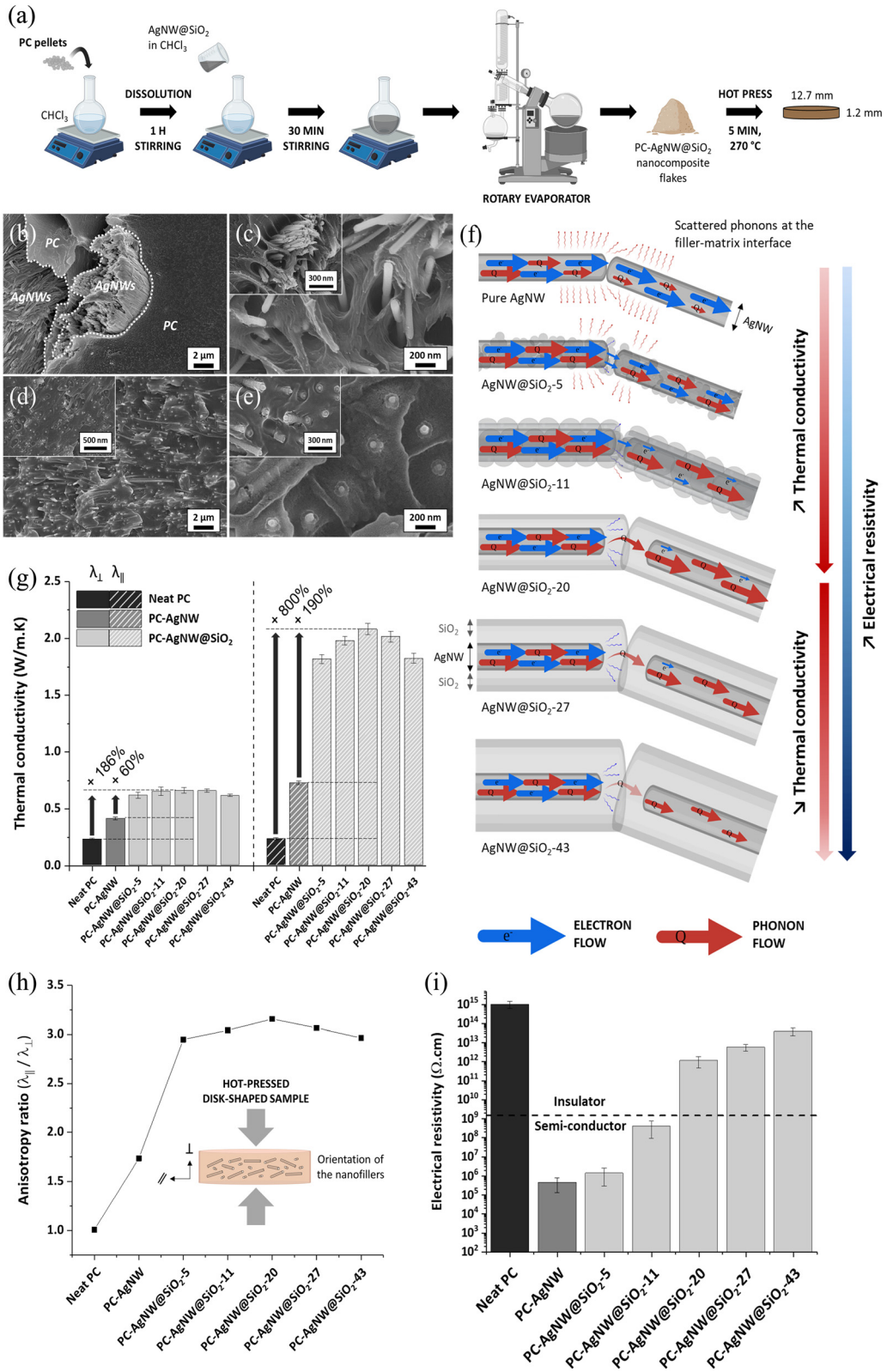

Fig. 2 (a) Synthesis process of PC-AgNW@SiO_2 nanocomposites. FE-SEM images of fractured surfaces of (b), (c) PC-AgNW and (d), (e) PC-AgNW@SiO_2 bulk samples. (f) Illustration showing the influence of the SiO_2 coating quality and thickness on electron and phonon flows at the interface of nanofillers embedded in the PC matrix. (g) Through-plane and in-plane thermal conductivity of bulk, hot-pressed samples at 25 °C and (h) thermal conductivity anisotropy ratio with an inset showing the orientation of the nanofillers in the plane perpendicular to the hot-pressing axis. (i) Electrical resistivity of PC nanocomposites filled with pure AgNW and AgNW@SiO_2 nanowires.

AgNWs or AgNW@SiO_2 nanofillers to the PC matrix did not affect its thermal stability, as observed from TGA curves displayed in Fig. S9 (ESI†). The onset of thermal degradation was around 400 °C for all samples and the residual mass increased slightly as the SiO_2 shell thickness increased.

Thermal conductivity of bulk, hot-pressed nanocomposites

Through-plane and in-plane thermal conductivity values of hot-pressed samples made of neat PC and nanocomposites are displayed in Fig. 2(g). Adding thermally conductive AgNWs to the PC matrix greatly improved the thermal conductivity of the resulting nanocomposite. Raw AgNWs increased the thermal conductivity in both through-plane and in-plane directions by 82% (up to 0.42 ± 0.01 W m^{-1} K^{-1}) and 213% (up to 0.73 ± 0.02 W m^{-1} K^{-1}) respectively. Silica-coated AgNWs further increased the thermal conductivity up to 0.66 ± 0.03 W m^{-1} K^{-1} and 2.08 ± 0.05 W m^{-1} K^{-1} for PC-AgNW@SiO_2-20, corresponding to thermal conductivity enhancements of 187% and 800% over neat PC and 60% and 190% over PC-AgNW, for through-plane and in-plane measurements respectively (see also Table S1, ESI†).

Such differences in thermal conductivity performances between through-plane and in-plane measurements are explained by one of the special features of the hot-press shaping process, which tends to orient 1D nanofillers in the perpendicular plane to the pressing direction. This induces higher in-plane thermal conductivity values and high thermal conductivity anisotropy ratios (Fig. 2(h)). The thermal conductivity results obtained in this work stand out from those found in the literature concerning thermally conductive and electrically insulating core–shell and ceramic fillers, as illustrated by the graph exhibited in Fig. S10 (ESI†).

The large increase in thermal conductivity for PC-AgNW@SiO_2 samples can be ascribed to the better dispersion of AgNW@SiO_2 core–shell nanowires and the enhanced interfacial compatibility with the PC matrix (Fig. 2(d) and (e)). The combined effects of these two phenomena create a high-performance thermally conductive network deeply anchored in the PC matrix. It is also supposed that the SiO_2 shell acts as an intermediate layer between the hard silver core and the soft PC matrix that alleviates the modulus mismatch at the filler–matrix interface. A high modulus mismatch is indeed responsible for high boundary thermal resistance and phonon scattering caused by vibration frequency incompatibilities existing between two atomically different phases (in this case the metallic AgNWs and the organic PC matrix). Since the thin SiO_2 ceramic shell has a modulus value falling between those of AgNWs and the polymer matrix,[32] it creates an easy-to-cross bridge for phonons at the interface, thus reducing their scattering[29,32,48] (Fig. 2(f)). An optimal SiO_2 thickness corresponding to the highest measured thermal conductivity has been determined to around 20 nm (PC-AgNW@SiO_2-20). For thinner thicknesses, the lower thermal conductivity is certainly due to an inferior coating quality as observed in FE-SEM images (Fig. 1(c) and (d)), detrimental to an efficient phonon transfer at the filler–matrix interface (Fig. S8b′ and c′, ESI†). It seems reasonable to assume that the decrease in thermal conductivity values measured on samples with a shell thickness above 20 nm can be explained by the combination of two factors. The first possible reason is associated with the low intrinsic thermal conductivity of the amorphous SiO_2 layer (≈1.5 W m^{-1} K^{-1}),[49] gradually reducing the group velocity of phonons throughout the interface (Fig. 2(f)). This decrease and reversing trend in thermal conductivity enhancement has already been observed in other different nanocomposite systems using thick SiO_2 shells in core–shell nanostructured nanofillers.[33,46,50,51] The second possible explanation for this drop in thermal conductivity at higher SiO_2 shell thicknesses is associated with a further increase of modulus mismatch. Indeed, previous studies have shown that the elastic modulus of thin film materials depends on the film thickness.[52–54] At low thicknesses (a few nanometers), the elastic modulus of the material decreases with thickness, which alleviates the modulus mismatch. Contrarily, thicker layers gradually get closer to the modulus of the bulk material, as thickness increases. This rationale has already been experimentally verified by two research groups studying the effect of a TiO_2 coating on AgNWs[52] and CuNWs.[28] Jiang *et al.*[52] found that a 30 nm thick TiO_2 coating on AgNWs had a detrimental effect on the thermal conductivity of an epoxy nanocomposite, resulting in lower performance than that obtained with pure AgNWs. By contrast, in the study of Ahn *et al.*,[28] the TiO_2 coating on CuNWs was ten times thinner. Under these circumstances, the modulus mismatch between the polymer matrix and CuNWs was lower and led to an increase of the thermal conductivity. The results obtained in the present study suggest that the low intrinsic thermal conductivity of SiO_2 and the increasing modulus mismatch associated with an increasing layer thickness would outweigh the good dispersion and the enhanced filler–matrix cohesion, reversing the trend in the thermal conductivity improvement. The temperature dependence of through-plane and in-plane thermal conductivities of the PC nanocomposites are shown in Fig. S11 (ESI†). As expected, thermal conductivity values rise slightly in a linear fashion from 25 °C to 125 °C, up to 2.29 ± 0.04 W m^{-1} K^{-1} for PC-AgNW@SiO_2-20 at 125 °C, which is attributed to the gradual increase in the specific heat capacity of the nanocomposite with temperature.

Electrical resistivity of PC nanocomposites

In addition to good thermal conductivity, the other essential property sought for PC nanocomposites is efficient electrical insulation. Any material is considered electrically insulating if its electrical resistivity surpasses 10^9 Ω cm.[7] Electrical resistivity values are displayed in Fig. 2(i). Not surprisingly, neat PC exhibited the highest electrical resistivity (1.02 ± 0.41 × 10^{15} Ω cm). However, adding only 3 vol% of pure AgNWs to the PC matrix boosted its electrical conductivity by almost 10 decades (the resistivity plummeted to 4.74 ± 3.40 × 10^5 Ω cm). On the other hand, the more the SiO_2 coating grows on the AgNW surface, the more the PC-AgNW@SiO_2 nanocomposite becomes resistive. More specifically, for PC-AgNW@SiO_2-5 and PC-AgNW@SiO_2-11 where the coatings did not cover the entire surface of AgNWs, leaving some gaps as illustrated in Fig. 2(f); it was found that electrical resistivity was not satisfactory. It was

only at thicknesses of 20 nm and above that the SiO_2 coating was fully effective (PC-AgNW@SiO_2-20 displayed an electrical resistivity of $1.13 \pm 0.68 \times 10^{12}$ Ω cm), providing complete and satisfying electrical insulation (Fig. 2(f) and (i)). Complementary electrical characterization including the measurements of the dielectric constant, dielectric loss and electrical conductivity as a function of frequency were performed (Fig. S12a and b, ESI†). Breakdown voltage characterization was also investigated (Fig. S12c and d, ESI†) and confirmed the beneficial effect of the SiO_2 shell on electrical performances of PC-AgNW@SiO_2 nanocomposites, which is in line with expectations for the nanostructures used in this work.

Thermal imaging

To assess the heat dissipation performance of PC nanocomposites, all samples, including neat PC, were subjected to a heating and a cooling cycle while their surface temperature was recorded live by using an infrared thermal imaging camera. Thermal images for heating and cooling processes are displayed in Fig. 3(a) and (b) respectively. Corresponding curves of surface temperature variation *vs.* time are presented in Fig. 3(c) and (d). PC nanocomposites exhibited significantly faster heating and cooling kinetics than neat PC, as highlighted by the calculated slope coefficients on each heating and cooling curves (see insets in Fig. 3(c) and (d)). This observation was

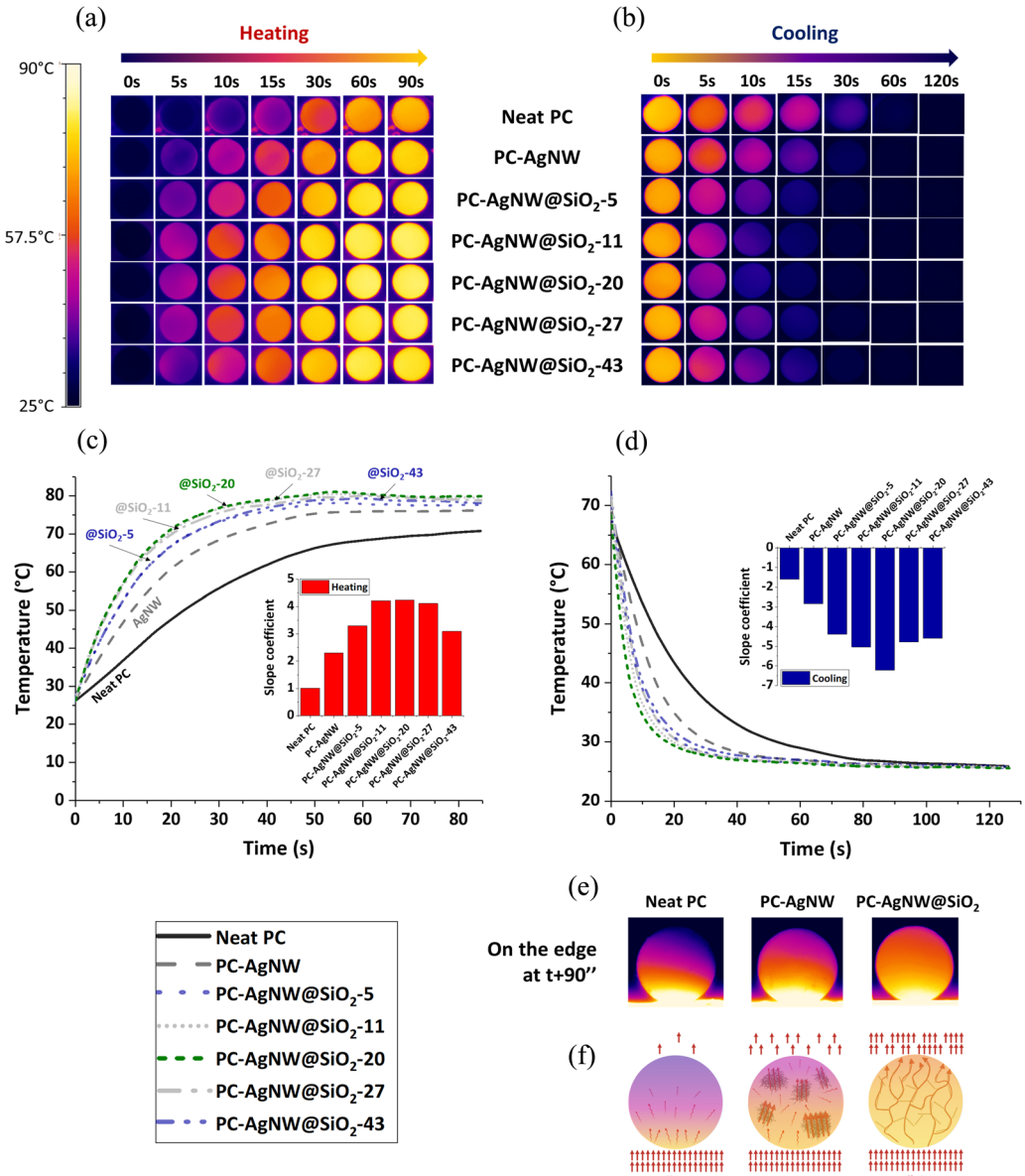

Fig. 3 Infrared thermal images of neat PC and PC nanocomposites during (a) heating and (b) cooling cycles; temperature variation over time during (c) heating and (d) cooling cycles. The insets in (c) and (d) correspond to the calculated slope coefficients for heating and cooling cycles respectively; (e) infrared thermal images of neat PC and PC nanocomposites during heating on the edge at t + 90 s and (f) illustration showing the construction of a high-performance thermally conductive network throughout the PC matrix using AgNW@SiO_2 nanofillers.

expected given the thermal conductivity results obtained previously. Interestingly, the calculated slope coefficient values on the heating and cooling curves followed the same trend as the thermal conductivity results, highlighting an optimum value for PC-AgNW@SiO_2-20. Among the different nanocomposites, those filled with AgNW@SiO_2 core–shell nanostructures were the fastest to heat up and to cool down, demonstrating once again their ability to dissipate heat more efficiently. Precisely, PC-AgNW@SiO_2-20 was the sample exhibiting the best heating and cooling performances. After heating for 30 s, it already reached 76 °C while PC-AgNW was only at 68 °C and neat PC at 55 °C (Fig. 3(c)). The temperature of the same sample dropped down to 29 °C after only 20 s of cooling from an initial surface temperature of 80 °C, whereas PC-AgNW was at 35 °C and neat PC at 43 °C (Fig. 3(d)). Thermal cycling performed on the edge of the disk-shaped samples revealed the existence of a pronounced thermal gradient in the in-plane direction for neat PC (Fig. 3(e)). The temperature distribution for PC-AgNW@SiO_2 nanocomposites was much better compared to other samples. The model depicted in Fig. 3(f) illustrates this observation through the formation of a high-performance thermally conductive network achieved by well-dispersed AgNW@SiO_2 nanofillers deeply anchored in the PC matrix. Therefore, PC nanocomposites with AgNW@SiO_2 nanowires, and especially the one using AgNW@SiO_2-20, exhibit better thermal exchange kinetics, resulting in superior cooling abilities.

Rheology

Rheological properties were assessed prior to filament extrusion and 3D printing attempts as the melt rheological properties of polymers are known to govern their flow behavior.[38,55] Fig. 4(c) displays the variations of the complex viscosity (η^*) of neat PC and PC-AgNW@SiO_2 nanocomposites at 250 °C as a function of the frequency. While neat PC exhibited an almost Newtonian behavior, PC-AgNW and PC-AgNW@SiO_2 nanocomposites showed a shear-thinning behavior, which is typical of polycarbonate loaded with 1D nanofillers.[56,57] Moreover, the viscosities of PC-AgNW@SiO_2 nanocomposites were higher than those of PC-AgNW over the entire frequency range and increased progressively with expanding SiO_2 layer thickness. These observations can be attributed to the stronger interfacial interaction between the AgNW@SiO_2 nanofillers and the PC matrix, as previously observed in FE-SEM images. The increasing SiO_2 thickness on AgNW surface is assumed to gradually restrain the polymer chain flow as well as the movement of the nanofillers in the nanocomposites, thereby increasing the viscosity. This can be ascribed to a higher contact surface area between the AgNW@SiO_2 nanofillers and the PC matrix, as the

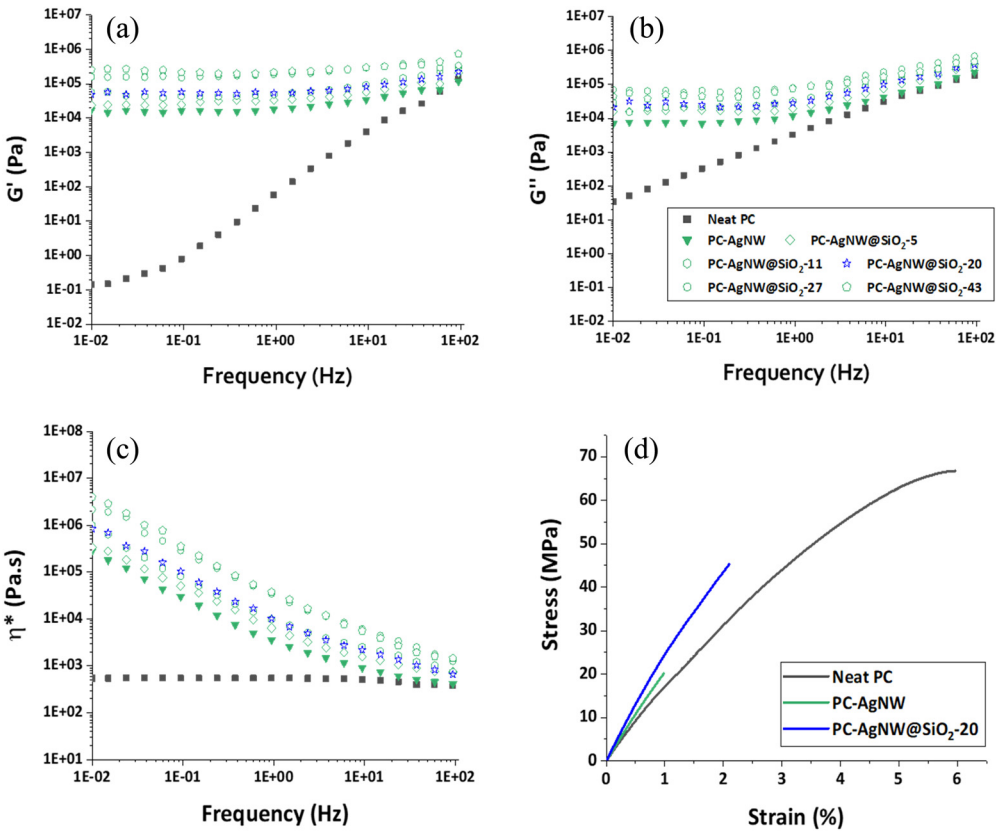

Fig. 4 (a)–(c) Rheological and (d) tensile properties of neat PC, PC-AgNW and PC-AgNW@SiO_2 nanocomposites: variations of (a) storage modulus, (b) loss modulus and (c) complex viscosity as a function of frequency at 250 °C; (d) averaged stress–strain curves of neat PC, PC-AgNW and PC-AgNW@SiO_2-20 nanocomposites.

surface to volume ratio increases very quickly for nanomaterials. For instance, AgNW@SiO_2-43 exhibits 40% more surface area than AgNW@SiO_2-20. The variations of storage modulus (G') and loss modulus (G'') of all samples as a function of frequency are displayed in Fig. 4(a) and (b). The variations of the damping factor $\tan\delta$ (G''/G') are presented in Fig. S13 (ESI†). The rheological behavior of the polymer melts was significantly altered by the presence of the nanofillers. The G' and G'' values of the nanocomposites increased significantly compared to those of pure PC. This increase is particularly marked at low frequency and more pronounced for the G' values. The presence of a plateau at low frequency for G' and G'' is correlated with the appearance of an apparent yield stress, resulting from the construction of an interconnected thermally conductive nanofiller network at only 3 vol% filler loading.[57,58] Among the PC-AgNW@SiO_2 nanocomposites, it was also observed that the higher the SiO_2 layer thickness, the higher the storage modulus values. This observation is also linked to the gradual restriction of the nanofiller mobility, restraining the long-range motion of the polycarbonate chains, thus stiffening the overall PC nanocomposite. Upon the addition of AgNW and AgNW@SiO_2 nanofillers in the PC matrix, tan δ values dropped close to zero as G' overpassed G'' over the entire frequency range, indicating a predominant elastic behavior for PC nanocomposites. More importantly, the rheological properties of PC-AgNW@SiO_2-20 and in particular its viscosity (blue star data points in Fig. 4(c)) were compatible with FDM 3D printer requirements.

Tensile properties

We chose to assess the mechanical properties of the nanocomposites using tensile tests on neat PC, PC-AgNW and PC-AgNW@SiO_2-20 loaded at 3 vol%, since PC-AgNW@SiO_2-20 achieved the best thermal conductivity results. Tensile measurement results are displayed as averaged stress–strain curves in Fig. 4(d). PC nanocomposites exhibited higher Young's modulus but lower tensile strengths and elongations at break than neat PC, as reported in Table S2 (ESI†). The addition of AgNWs to the PC matrix increases its stiffness but also weakens the overall structure. However, AgNW@SiO_2-20 core–shell nanowires lead to better tensile strength and elongation at break than pure AgNWs, and even better Young's modulus. Consequently, PC-AgNW@SiO_2-20 nanocomposites are stiffer than PC-AgNW, but also stronger and tougher. This is again a direct consequence of the enhanced filler–matrix interfacial adhesion while using silica-coated AgNW nanofillers. Mechanical specifications are obviously application dependent, satisfyingly the obtained values reported in Table S2 (ESI†) meet the expected ones for battery casing which was the first targeted application.

3D printing of AgNW@SiO_2-20 nanocomposites

1D nanofillers are known to give anisotropic properties due to their high aspect ratio. To make the most of this anisotropy, the nanofillers can be oriented into a certain direction to maximize the thermal conductivity. The FDM process has become one of the most popular 3D printing techniques owing to its easy set-up and low cost. One of the distinctive features of 3D printing of polymer nanocomposites using FDM is that nanofillers tend to align in the printing direction.[59,60] 3D printed test specimens are presented in Fig. S14 (ESI†). Neat PC and PC-AgNW@SiO_2-20 specimens were both printed in 0°/0° unidirectional and 0°/90° criss-cross successive layers (Fig. 5(a)) through a 0.4 mm heated nozzle moving in the (x,y) plane (Fig. 5(b)). Several cuts were performed on each disk-shaped punched sample to analyze the process-related microstructural arrangement of the nanocomposite, in both unidirectional and criss-cross printing directions (Fig. 5(a) and (c)). The different cutting styles are schematically presented in Fig. 5(c). For the 0°/0° unidirectional print, one cut parallel (1) and another perpendicular (2) to the printing direction were performed (Fig. 5(c_1) and (c_2)). For the 0°/90° criss-cross print, a normal cut (3) and a 45° cut (4) were done (Fig. 5(c_3) and (c_4)). Associated FE-SEM images are presented in Fig. 5(d_1)–(d_4). Insets show the stacking orientation of the successive 3D printed layers for each cut through lower magnification images. The high-magnification FE-SEM images clearly show the orientation and alignment of all AgNW@SiO_2-20 nanofillers in the same direction which corresponds to the printing direction (represented as yellow arrows or arrowheads (Fig. 5(d)). The thermal conductivity properties associated with this orientation were then measured through-plane and in-plane for each sample. The results are presented in Fig. 5(e) and compared with bulk properties. The thermal conductivity of neat PC was not affected by the 3D printing process, neither in the through-plane nor in the in-plane directions. Interestingly, the through-plane thermal conductivities (z direction) of PC-AgNW@SiO_2-20 decreased in both unidirectional and criss-cross printing directions compared to the hot-pressed bulk sample. This can be explained by the fact that almost all nanofillers were oriented in the (x,y) plane, which is perpendicular to the through-plane thermal diffusivity testing direction (z), either in the unidirectional or in the criss-cross sample. This was not the case for bulk samples, where some nanofillers remained oriented in the testing direction after hot-pressing (random orientation).

This loss in through-plane thermal conductivity can also be attributed to the formation of voids between the printed layers (some are visible in Fig. 5(d_3) and (d_4)) which are responsible for creating macroscopic thermal contact resistances at the interface of two successive layers.[61] However, the orientation and alignment of AgNW@SiO_2-20 in the 3D printed PC nanocomposites have a major influence on in-plane measurements. The 0/0 perpendicular cut (2) exhibited the best thermal conductivity, up to 3.48 ± 0.06 W m^{-1} K^{-1}, since all AgNW@SiO_2-20 nanofillers were aligned in the testing direction. This corresponds to a fifteen-fold increase in thermal conductivity with regard to neat PC. The alignment of the nanofillers in the printing direction is therefore responsible for very high anisotropy ratios (Fig. 5(e)). As expected, the 0/0 parallel cut (1) showed the lowest in-plane thermal conductivity (0.81 ± 0.01 W m^{-1} K^{-1}), since all the nanofillers were 90°-oriented regarding the in-plane testing direction. Interestingly, it was still 2.5 times higher than the

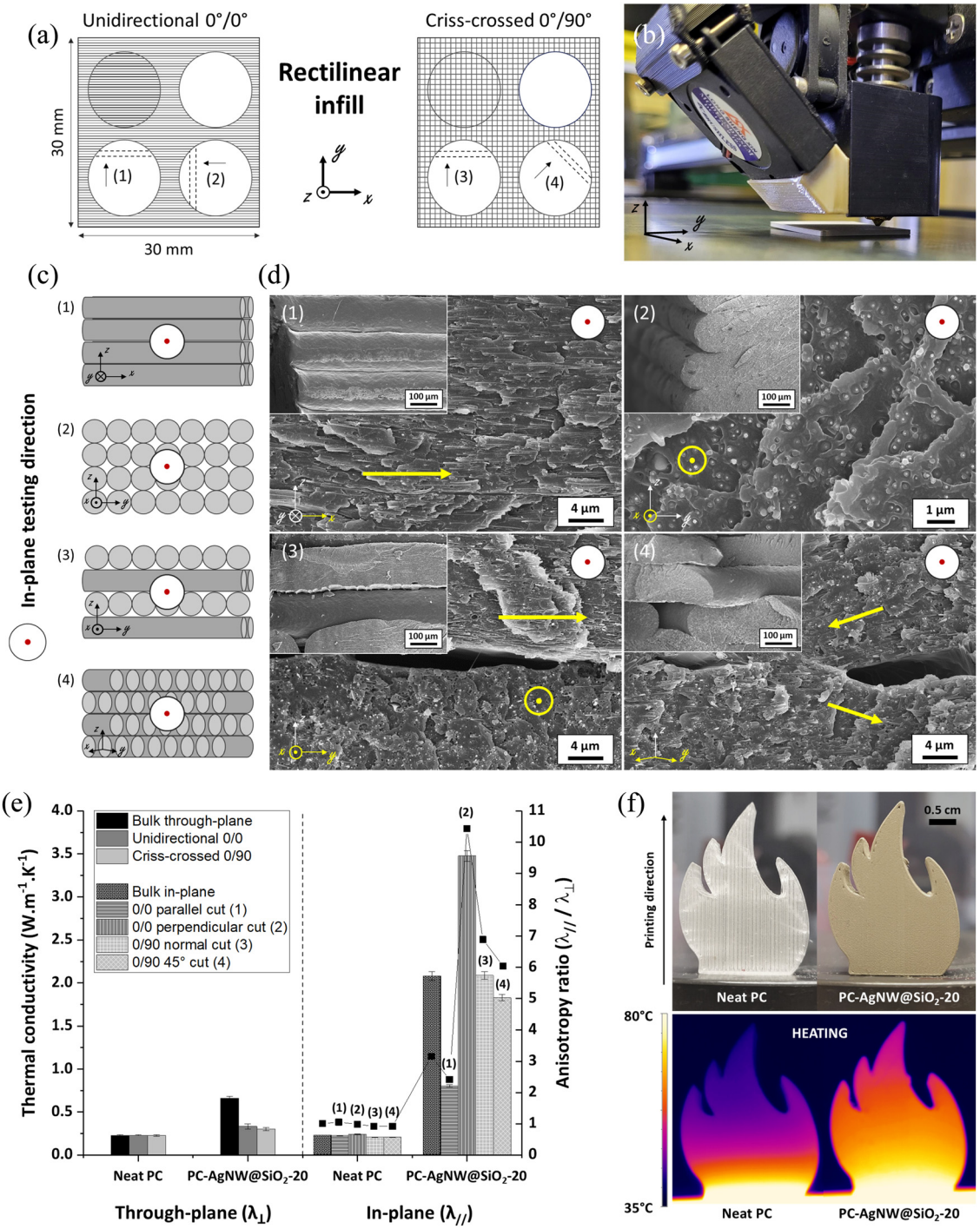

Fig. 5 (a) Printing patterns for test specimen filled with a rectilinear infill; (b) picture of the print head and the printing nozzle used in this work; (c) cross-sectional cutting styles: (c_1) 0/0 parallel cut, (c_2) 0/0 perpendicular cut, (c_3) 0/90 normal cut and (c_4) 0/90 45° cut; (d) corresponding FE-SEM images of (d_1) 0/0 parallel cut, (d_2) 0/0 perpendicular cut, (d_3) 0/90 normal cut and (d_4) 0/90 45° cut. The yellow arrows and arrowheads indicate the printing direction. (e) Through-plane and in-plane thermal conductivity along with corresponding anisotropy ratios of bulk and 3D printed neat PC and PC-AgNW@SiO_2-20 nanocomposite as a function of the printing raster angle and in-plane cutting style; (f) 3D printed demo parts of neat PC and PC-AgNW@SiO_2-20 with corresponding thermal images during the heating cycle (150 s in).

through-plane thermal conductivity of the unidirectional sample (0.33 ± 0.03 W m^{-1} K^{-1}), even though the nanofillers were oriented in the same directions for both samples. This can be explained by a higher amount of interstitial voids between layers in the through-plane direction compared to the in-plane direction. Indeed, as the asymmetry of the printing beads is very high due to a higher extrusion width compared to the layer height (width/height ratio ≈ 4), there are in this case more layers (*i.e.* interfaces)

in the through-plane direction than in the (x,y) plane. More interfaces mean more voids, resulting in higher macroscopic interfacial thermal resistance. The 0/90 normal cut (3) in-plane thermal conductivity was found to be about the same as that of the bulk sample and intermediate between the in-plane values of the 0/0 parallel cut (1) and 0/0 perpendicular cut (2). This observation was expected since the 0/90 normal cut (Fig. 5(d_3)) is a perfectly balanced mix between the 0/0 parallel cut (Fig. 5(d_1)) and the 0/0 perpendicular cut (Fig. 5(d_2)). This also demonstrates that the random orientation of the nanofillers in the bulk could be modeled by a balanced alternation of unidirectional layer orientations, since the thermal conductivity measured in both cases is equivalent. As for the 0/90 45° cut, its in-plane thermal conductivity value was relatively close to that of the 0/90 normal cut, although slightly lower. The thermal conductivity values obtained in this work compare well to the results found in the literature for 3D printable, thermally conductive, and electrically insulating polymer nanocomposites (Table S3, ESI†). To our knowledge, the original approach described herein delivers the best results to date (Fig. S15, ESI†). Fig. 5(f) displays a proof of concept, constructed with both neat PC and PC-AgNW@SiO_2-20 and 3D printed with a rectilinear, unidirectional infill from base to top. Thermal imaging revealed thermal gradients for both composition and highlighted the superior heat dissipation and cooling abilities of the PC-AgNW@SiO_2-20 nanocomposite (Fig. S16, ESI†). The orientation and alignment of 1D nanofillers can be a serious advantage if they are controlled and if the design of anisotropic parts is properly thought out. The properties of manufactured devices can thus be finely tuned and optimized by aligning the extrusion orientation with the desired preferential direction maximizing the heat dissipation properties.

Conclusions

AgNW@SiO_2 core–shell nanostructures with continuous and conformal SiO_2 nanolayers of controlled thicknesses ranging from 5 to 43 nm have been successfully synthesized. Their use as thermally conductive and electrically insulating nanofillers to improve heat dissipation performances of a PC matrix was demonstrated, and the fabrication of 3D printable nanocomposite filaments at 3 vol% loading was achieved. This is, to the best of our knowledge, the first time that thermally conductive and electrically insulating polymer nanocomposites filled with core–shell 1D nanofillers are successfully 3D printed by FDM.

The silica nanolayer not only preserves the electrical insulation of the PC matrix thanks to the SiO_2 intrinsic properties, but also greatly improves the thermal conductivity of bulk PC nanocomposites (up to 2.08 ± 0.05 W m^{-1} K^{-1} at 3 vol% loading, a 190% and 800% improvement over PC-AgNW and neat PC, respectively). This dramatic thermal conductivity enhancement is attributed to a greatly improved filler–matrix cohesion and a much better distribution in the PC matrix.

The influence of the manufacturing process on thermal and electrical properties was also investigated. The most promising nanocomposite was 3D printed using the FDM technique. The resulting orientation and alignment of the nanofillers provided by the 3D printing technique led to remarkable in-plane thermal conductivities, up to 3.48 ± 0.06 W m^{-1} K^{-1} for the PC-AgNW@SiO_2-20 nanocomposite, while keeping the material electrically insulating (electrical resistivity $>10^{12}$ Ω cm). This corresponds to a fifteen-fold increase in thermal conductivity with regard to the neat PC.

We thus demonstrate that the development of advanced core–shell nanowires can successfully lead to the 3D printing of high-performance and anisotropically controlled thermally conductive yet electrically insulating advanced materials. We believe this is a promising route to meet the ever-more challenging industrial needs for thermal management and on demand manufacturing of future heat dissipation devices.

Experimental section

Materials

Silver nanowires (AgNW dispersion in isopropanol at 30 g kg^{-1}, diameter = 70 ± 5 nm, length = 10 ± 2 μm) were purchased from Protavic International (France). Tetraethyl orthosilicate (TEOS, 98.0%), ammonium hydroxide solution (NH_4OH, 28.0–30.0%) and chloroform ($CHCl_3$, 99.0%) were purchased from Sigma-Aldrich (USA). Anhydrous EtOH was supplied by Carlo Erba (Germany). Polycarbonate (PC, grade Makrolon LED2245) was purchased from Covestro (Germany). Polytetrafluoroethylene (PTFE) membrane filters with a pore size of 1.2 μm were purchased from Sartorius (Germany).

Synthesis of AgNW@SiO_2 core–shell nanostructures

Silica-coated silver nanowires (AgNW@SiO_2) were synthetized through a flexible sol–gel approach.[62–64] The whole AgNW@SiO_2 synthesis procedure is detailed in the ESI† and summarized in the scheme displayed in Fig. 1(a).

Preparation of PC-AgNW@SiO_2 nanocomposites

PC-AgNW@SiO_2 nanocomposites were synthetized by the solution mixing technique. Samples were prepared in order to obtain a 3 vol% loading rate of AgNW@SiO_2 in the polycarbonate matrix. Details about the preparation of the PC-AgNW@SiO_2 bulk nanocomposites can be found in the ESI.† The disk-shaped samples were obtained by hot pressing the flakes in a pressing die under an uniaxial hot press set at 270 °C (Carver 30T 4128, Carver Inc., USA). The nanocomposite synthesis process is summarized in the scheme presented in Fig. 2(a). Note that PC-AgNW bulk nanocomposites with pure AgNWs were prepared as control samples. For shaping PC-AgNW@SiO_2 nanocomposites in filament form, a similar process was employed as described in the ESI† and Fig. S1.

3D printing of neat PC and PC-AgNW@SiO_2 nanocomposite filaments

3D printing was carried out using an open source 3D printer (Hydra 16A, Hyrel 3D, USA). Details of the procedure can be found in the ESI† file.

Characterization

Characterization detailed methods are gathered in the ESI.† In particular, thermal conductivity values (λ) were calculated using the formula $\lambda = \alpha \times \rho \times C_p$, where α is the measured thermal diffusivity, ρ is the measured bulk density and C_p is the measured specific heat capacity.

Data availability

The data supporting this article have been included as part of the ESI.†

Conflicts of interest

There are no conflicts to declare.

Acknowledgements

The authors acknowledge C. Brouard for helping in the silver titration experiments and analysis, A. Benayad for helping in the XPS characterization and M. Bey for helping in the breakdown voltage measurements. This work was supported by the Agence de l'Innovation de Defense (AID, France) through a PhD grant to Antoine Bodin.

References

1 Z. Meng, Z. Dai, K. Chen and S. Wang, Investigation on Preparation, Thermal, and Mechanical Properties of Carbon Fiber Decorated with Hexagonal Boron Nitride/Silicone Rubber Composites for Battery Thermal Management, *Int. J. Energy Res.*, 2021, **45**(3), 4396–4409, DOI: **10.1002/er.6110**.

2 A. L. Moore and L. Shi, Emerging Challenges and Materials for Thermal Management of Electronics, *Mater. Today*, 2014, **17**(4), 163–174, DOI: **10.1016/j.mattod.2014.04.003**.

3 K. Liu, Y. Liu, D. Lin, A. Pei and Y. Cui, Materials for Lithium-Ion Battery Safety, *Sci. Adv.*, 2018, **4**(6), eaas9820, DOI: **10.1126/sciadv.aas9820**.

4 Y. Zhu, J. Xie, A. Pei, B. Liu, Y. Wu, D. Lin, J. Li, H. Wang, H. Chen, J. Xu, A. Yang, C.-L. Wu, H. Wang, W. Chen and Y. Cui, Fast Lithium Growth and Short Circuit Induced by Localized-Temperature Hotspots in Lithium Batteries, *Nat. Commun.*, 2019, **10**(1), 2067, DOI: **10.1038/s41467-019-09924-1**.

5 X. Feng, M. Ouyang, X. Liu, L. Lu, Y. Xia and X. He, Thermal Runaway Mechanism of Lithium Ion Battery for Electric Vehicles: A Review, *Energy Storage Mater.*, 2018, **10**, 246–267, DOI: **10.1016/j.ensm.2017.05.013**.

6 S. Anandan and V. Ramalingam, Thermal Management of Electronics: A Review of Literature, *Therm. Sci.*, 2008, **12**(2), 5–26, DOI: **10.2298/TSCI0802005A**.

7 C. Zhao, Y. Li, Y. Liu, H. Xie and W. Yu, A Critical Review of the Preparation Strategies of Thermally Conductive and Electrically Insulating Polymeric Materials and Their Applications in Heat Dissipation of Electronic Devices, *Adv. Compos. Hybrid Mater.*, 2022, **6**(1), 27, DOI: **10.1007/s42114-022-00584-2**.

8 L. H. Saw, Y. Ye and A. A. O. Tay, Feasibility Study of Boron Nitride Coating on Lithium-Ion Battery Casing, *Appl. Therm. Eng.*, 2014, **73**(1), 154–161, DOI: **10.1016/j.applthermaleng.2014.06.061**.

9 Q. Wang and Y. Li, Research Advances in Preparation, Mechanism and Application of Thermally Conductive and Electrically Insulating Polymer Composites in Thermal Management Materials: A Review, *High Perform. Polym.*, 2023, 09540083231164342, DOI: **10.1177/09540083231164342**.

10 H. Chen, V. V. Ginzburg, J. Yang, Y. Yang, W. Liu, Y. Huang, L. Du and B. Chen, Thermal Conductivity of Polymer-Based Composites: Fundamentals and Applications, *Prog. Polym. Sci.*, 2016, **59**, 41–85, DOI: **10.1016/j.progpolymsci.2016.03.001**.

11 Z. Han and A. Fina, Thermal Conductivity of Carbon Nanotubes and Their Polymer Nanocomposites: A Review, *Prog. Polym. Sci.*, 2011, **36**(7), 914–944, DOI: **10.1016/j.progpolymsci.2010.11.004**.

12 Ye Mamunya, A. Boudenne, N. Lebovka, L. Ibos, Y. Candau and M. Lisunova, Electrical and Thermophysical Behaviour of PVC-MWCNT Nanocomposites, *Compos. Sci. Technol.*, 2008, **68**(9), 1981–1988, DOI: **10.1016/j.compscitech.2007.11.014**.

13 S. Stankovich, D. A. Dikin, G. H. B. Dommett, K. M. Kohlhaas, E. J. Zimney, E. A. Stach, R. D. Piner, S. T. Nguyen and R. S. Ruoff, Graphene-Based Composite Materials, *Nature*, 2006, **442**(7100), 282–286, DOI: **10.1038/nature04969**.

14 I. Krupa, I. Novák and I. Chodák, Electrically and Thermally Conductive Polyethylene/Graphite Composites and Their Mechanical Properties, *Synth. Met.*, 2004, **145**(2), 245–252, DOI: **10.1016/j.synthmet.2004.05.007**.

15 S. Wang, Y. Cheng, R. Wang, J. Sun and L. Gao, Highly Thermal Conductive Copper Nanowire Composites with Ultralow Loading: Toward Applications as Thermal Interface Materials, *ACS Appl. Mater. Interfaces*, 2014, **6**(9), 6481–6486, DOI: **10.1021/am500009p**.

16 K. Pashayi, H. R. Fard, F. Lai, S. Iruvanti, J. Plawsky and T. Borca-Tasciuc, Self-Constructed Tree-Shape High Thermal Conductivity Nanosilver Networks in Epoxy, *Nanoscale*, 2014, **6**(8), 4292–4296, DOI: **10.1039/C3NR06494H**.

17 S. Kume, I. Yamada, K. Watari, I. Harada and K. Mitsuishi, High-Thermal-Conductivity AlN Filler for Polymer/Ceramics Composites, *J. Am. Ceram. Soc.*, 2009, **92**(s1), S153–S156, DOI: **10.1111/j.1551-2916.2008.02650.x**.

18 Y. Yao, X. Zeng, K. Guo, R. Sun and J. Xu, The Effect of Interfacial State on the Thermal Conductivity of Functionalized Al_2O_3 Filled Glass Fibers Reinforced Polymer Composites, *Composites, Part A*, 2015, **69**, 49–55, DOI: **10.1016/j.compositesa.2014.10.027**.

19 A. Bodin, T. Pietri and J.-P. Simonato, Mild Air Oxidation of Boron Nitride Nanotubes. Application as Nanofillers for Thermally Conductive Polycarbonate Nanocomposites,

Nanotechnology, 2023, **34**(12), 125601, DOI: **10.1088/1361-6528/acae2b**.

20 Ye. P. Mamunya, V. V. Davydenko, P. Pissis and E. V. Lebedev, Electrical and Thermal Conductivity of Polymers Filled with Metal Powders, *Eur. Polym. J.*, 2002, **38**(9), 1887–1897, DOI: **10.1016/S0014-3057(02)00064-2**.

21 P. F. Flowers, C. Reyes, S. Ye, M. J. Kim and B. J. Wiley, 3D Printing Electronic Components and Circuits with Conductive Thermoplastic Filament, *Addit. Manuf.*, 2017, **18**, 156–163, DOI: **10.1016/j.addma.2017.10.002**.

22 R. H. Sanatgar, A. Cayla, C. Campagne and V. Nierstrasz, Morphological and Electrical Characterization of Conductive Polylactic Acid Based Nanocomposite before and after FDM 3D Printing, *J. Appl. Polym. Sci.*, 2019, **136**(6), 47040, DOI: **10.1002/app.47040**.

23 Y. Guo, K. Ruan, X. Shi, X. Yang and J. Gu, Factors Affecting Thermal Conductivities of the Polymers and Polymer Composites: A Review, *Compos. Sci. Technol.*, 2020, **193**, 108134, DOI: **10.1016/j.compscitech.2020.108134**.

24 R. Qian, J. Yu, C. Wu, X. Zhai and P. Jiang, Alumina-Coated Graphene Sheet Hybrids for Electrically Insulating Polymer Composites with High Thermal Conductivity, *RSC Adv.*, 2013, **3**(38), 17373–17379, DOI: **10.1039/C3RA42104J**.

25 W. Yan, Y. Zhang, H. Sun, S. Liu, Z. Chi, X. Chen and J. Xu, Polyimide Nanocomposites with Boron Nitride-Coated Multi-Walled Carbon Nanotubes for Enhanced Thermal Conductivity and Electrical Insulation, *J. Mater. Chem. A*, 2014, **2**(48), 20958–20965, DOI: **10.1039/C4TA04663C**.

26 D. Mao, J. Chen, L. Ren, K. Zhang, M. M. F. Yuen, X. Zeng, R. Sun, J.-B. Xu and C.-P. Wong, Spherical Core–Shell Al@Al_2O_3 Filled Epoxy Resin Composites as High-Performance Thermal Interface Materials, *Composites, Part A*, 2019, **123**, 260–269, DOI: **10.1016/j.compositesa.2019.05.024**.

27 Z. Wang, Y. Zhang, J. Yi, N. Cai and J. Guo, Core-Shell Cu@Al_2O_3 Fillers for Enhancing Thermal Conductivity and Retaining Electrical Insulation of Epoxy Composites, *J. Alloys Compd.*, 2022, **928**, 167123, DOI: **10.1016/j.jallcom.2022.167123**.

28 K. Ahn, K. Kim and J. Kim, Thermal Conductivity and Electric Properties of Epoxy Composites Filled with TiO_2-Coated Copper Nanowire, *Polymer*, 2015, **76**, 313–320, DOI: **10.1016/j.polymer.2015.09.001**.

29 W. Cui, F. Du, J. Zhao, W. Zhang, Y. Yang, X. Xie and Y.-W. Mai, Improving Thermal Conductivity While Retaining High Electrical Resistivity of Epoxy Composites by Incorporating Silica-Coated Multi-Walled Carbon Nanotubes, *Carbon*, 2011, **49**(2), 495–500, DOI: **10.1016/j.carbon.2010.09.047**.

30 C. Shen, H. Wang, T. Zhang and Y. Zeng, Silica Coating onto Graphene for Improving Thermal Conductivity and Electrical Insulation of Graphene/Polydimethylsiloxane Nanocomposites, *J. Mater. Sci. Technol.*, 2019, **35**(1), 36–43, DOI: **10.1016/j.jmst.2018.09.016**.

31 Y. Zhou, L. Wang, H. Zhang, Y. Bai, Y. Niu and H. Wang, Enhanced High Thermal Conductivity and Low Permittivity of Polyimide Based Composites by Core–Shell Ag@SiO_2 Nanoparticle Fillers, *Appl. Phys. Lett.*, 2012, **101**(1), 012903, DOI: **10.1063/1.4733324**.

32 C. Chen, Y. Tang, Y. S. Ye, Z. Xue, Y. Xue, X. Xie and Y.-W. Mai, High-Performance Epoxy/Silica Coated Silver Nanowire Composites as Underfill Material for Electronic Packaging, *Compos. Sci. Technol.*, 2014, **105**, 80–85, DOI: **10.1016/j.compscitech.2014.10.002**.

33 K. Kim, K. Ahn, H. Ju and J. Kim, Improvement of Insulating and Thermal Properties of SiO_2-Coated Copper Nanowire Composites, *Ind. Eng. Chem. Res.*, 2016, **55**(10), 2713–2720, DOI: **10.1021/acs.iecr.5b04141**.

34 S. Zhang, X. Y. Cao, Y. M. Ma, Y. C. Ke, J. K. Zhang and F. S. Wang, The Effects of Particle Size and Content on the Thermal Conductivity and Mechanical Properties of Al_2O_3/High Density Polyethylene (HDPE) Composites, *eXPRESS Polym. Lett.*, 2011, **5**(7), 581–590, DOI: **10.3144/expresspolymlett.2011.57**.

35 L. Rivière, A. Lonjon, E. Dantras, C. Lacabanne, P. Olivier and N. R. Gleizes, Silver Fillers Aspect Ratio Influence on Electrical and Thermal Conductivity in PEEK/Ag Nanocomposites, *Eur. Polym. J.*, 2016, **85**, 115–125, DOI: **10.1016/j.eurpolymj.2016.08.003**.

36 N. Burger, A. Laachachi, M. Ferriol, M. Lutz, V. Toniazzo and D. Ruch, Review of Thermal Conductivity in Composites: Mechanisms, Parameters and Theory, *Prog. Polym. Sci.*, 2016, **61**, 1–28, DOI: **10.1016/j.progpolymsci.2016.05.001**.

37 T. Pietri, B. J. Wiley and J.-P. Simonato, Boron Nitride Nanotubes for Heat Dissipation in Polycaprolactone Composites, *ACS Appl. Nano Mater.*, 2021, **4**(5), 4774–4780, DOI: **10.1021/acsanm.1c00365**.

38 S. Bakrani Balani, F. Chabert, V. Nassiet and A. Cantarel, Influence of Printing Parameters on the Stability of Deposited Beads in Fused Filament Fabrication of Poly(Lactic) Acid, *Addit. Manuf.*, 2019, **25**, 112–121, DOI: **10.1016/j.addma.2018.10.012**.

39 A. D. Valino, J. R. C. Dizon, A. H. Espera, Q. Chen, J. Messman and R. C. Advincula, Advances in 3D Printing of Thermoplastic Polymer Composites and Nanocomposites, *Prog. Polym. Sci.*, 2019, **98**, 101162, DOI: **10.1016/j.progpolymsci.2019.101162**.

40 Y. Zhou and F. Liu, High-Performance Polyimide Nanocomposites with Core–Shell AgNWs@BN for Electronic Packagings, *Appl. Phys. Lett.*, 2016, **109**(8), 082901, DOI: **10.1063/1.4961625**.

41 M. Yang, X. Wang, R. Wang and S. Qi, The Fabrication and Thermal Conductivity of Epoxy Composites with 3D Nanofillers of AgNWs@SiO2&GNPs, *J. Mater. Sci.: Mater. Electron.*, 2017, **28**(21), 16141–16147, DOI: **10.1007/s10854-017-7514-1**.

42 H. Gan, Y. Zhang, S. Li, W. Zhu, J. Wang and Z. Xue, Synergetic Effects of Silica-Coated Silver Nanowires in Composite Single-Ion Conducting Polymer Electrolytes for Lithium Metal Batteries, *J. Power Sources*, 2022, **551**, 232171, DOI: **10.1016/j.jpowsour.2022.232171**.

43 M. Rothe, Y. Zhao, G. Kewes, Z. Kochovski, W. Sigle, P. A. van Aken, C. Koch, M. Ballauff, Y. Lu and O. Benson,

Silver Nanowires with Optimized Silica Coating as Versatile Plasmonic Resonators, *Sci. Rep.*, 2019, **9**, 3859, DOI: 10.1038/s41598-019-40380-5.

44 Y. Sun, Y. Yin, B. T. Mayers, T. Herricks and Y. Xia, Uniform Silver Nanowires Synthesis by Reducing $AgNO_3$ with Ethylene Glycol in the Presence of Seeds and Poly(Vinyl Pyrrolidone), *Chem. Mater.*, 2002, **14**(11), 4736–4745, DOI: 10.1021/cm020587b.

45 Y. Sun and Y. Xia, Large-Scale Synthesis of Uniform Silver Nanowires Through a Soft, Self-Seeding, Polyol Process, *Adv. Mater.*, 2002, **14**(11), 833–837, DOI: 10.1002/1521-4095(20020605)14:11<833::AID-ADMA833>3.0.CO;2-K.

46 S. Choi, K. Kim, J. Nam and S. E. Shim, Synthesis of Silica-Coated Graphite by Enolization of Polyvinylpyrrolidone and Its Thermal and Electrical Conductivity in Polymer Composites, *Carbon*, 2013, **60**, 254–265, DOI: 10.1016/j.carbon.2013.04.034.

47 L. Fang, Y. Yan, O. Agarwal, J. E. Seppala, K. J. Hemker and S. H. Kang, Processing-Structure-Property Relationships of Bisphenol-A-Polycarbonate Samples Prepared by Fused Filament Fabrication, *Addit. Manuf.*, 2020, **35**, 101285, DOI: 10.1016/j.addma.2020.101285.

48 Y. Tang, C. Xiao, J. Ding, K. Hu, K. Zheng and X. Tian, Synergetic Enhancement of Thermal Conductivity in the Silica-Coated Boron Nitride (SiO2@BN)/Polymethyl Methacrylate (PMMA) Composites, *Colloid Polym. Sci.*, 2020, **298**(4–5), 385–393, DOI: 10.1007/s00396-020-04617-4.

49 G. Wypych, *Handbook of Fillers*, Elsevier, Toronto, Canada, 2016.

50 Y. Liang, B. Liu, B. Zhang, Z. Liu and W. Liu, Effects and Mechanism of Filler Surface Coating Strategy on Thermal Conductivity of Composites: A Case Study on Epoxy/SiO_2-Coated BN Composites, *Int. J. Heat Mass Transf.*, 2021, **164**, 120533, DOI: 10.1016/j.ijheatmasstransfer.2020.120533.

51 Y. Kim, M. Kim, H.-G. Seong, J. Y. Jung, S.-H. Baeck and S. E. Shim, Roles of Silica-Coated Layer on Graphite for Thermal Conductivity, Heat Dissipation, Thermal Stability, and Electrical Resistivity of Polymer Composites, *Polymer*, 2018, **148**, 295–302, DOI: 10.1016/j.polymer.2018.06.056.

52 Y. Jiang, M. Li, C. Chen, Z. Xue, X. Xie, X. Zhou and Y.-W. Mai, Effect of Elastic Modulus Mismatch of Epoxy/Titanium Dioxide Coated Silver Nanowire Composites on the Performance of Thermal Conductivity, *Compos. Sci. Technol.*, 2018, **165**, 206–213, DOI: 10.1016/j.compscitech.2018.06.028.

53 L. Zhu and X. Zheng, Influence of Interface Energy and Grain Boundary on the Elastic Modulus of Nanocrystalline Materials, *Acta Mech.*, 2010, **213**(3), 223–234, DOI: 10.1007/s00707-009-0263-3.

54 R. Dingreville, J. Qu and C. Mohammed, Surface Free Energy and Its Effect on the Elastic Behavior of Nano-Sized Particles, Wires and Films, *J. Mech. Phys. Solids*, 2005, **53**(8), 1827–1854, DOI: 10.1016/j.jmps.2005.02.012.

55 A. Das, E. L. Gilmer, S. Biria and M. J. Bortner, Importance of Polymer Rheology on Material Extrusion Additive Manufacturing: Correlating Process Physics to Print Properties, *ACS Appl. Polym. Mater.*, 2021, **3**(3), 1218–1249, DOI: 10.1021/acsapm.0c01228.

56 M. Abdel-Goad and P. Pötschke, Rheological Characterization of Melt Processed Polycarbonate-Multiwalled Carbon Nanotube Composites, *J. Non-Newton. Fluid Mech.*, 2005, **128**(1), 2–6, DOI: 10.1016/j.jnnfm.2005.01.008.

57 S. Abbasi, P. J. Carreau, A. Derdouri and M. Moan, Rheological Properties and Percolation in Suspensions of Multiwalled Carbon Nanotubes in Polycarbonate, *Rheol. Acta*, 2009, **48**(9), 943–959, DOI: 10.1007/s00397-009-0375-7.

58 Y. Bai, S. Zhou, X. Lei, H. Zou and M. Liang, Enhanced Thermal Conductivity of Polycarbonate-Based Composites by Constructing a Dense Filler Packing Structure Consisting of Hybrid Boron Nitride and Flake Graphite, *J. Appl. Polym. Sci.*, 2022, **139**(37), e52895, DOI: 10.1002/app.52895.

59 Y. Jia, H. He, Y. Geng, B. Huang and X. Peng, High Through-Plane Thermal Conductivity of Polymer Based Product with Vertical Alignment of Graphite Flakes Achieved via 3D Printing, *Compos. Sci. Technol.*, 2017, **145**, 55–61, DOI: 10.1016/j.compscitech.2017.03.035.

60 T. Mulholland, S. Goris, J. Boxleitner, T. A. Osswald and N. Rudolph, Process-Induced Fiber Orientation in Fused Filament Fabrication, *J. Compos. Sci.*, 2018, **2**(3), 45, DOI: 10.3390/jcs2030045.

61 H. Prajapati, D. Ravoori, R. L. Woods and A. Jain, Measurement of Anisotropic Thermal Conductivity and Inter-Layer Thermal Contact Resistance in Polymer Fused Deposition Modeling (FDM), *Addit. Manuf.*, 2018, **21**, 84–90, DOI: 10.1016/j.addma.2018.02.019.

62 X. Zhuang, Y. Zhou and F. Liu, A Novel 3D Sandwich Structure of Hybrid Graphite Nanosheets and Silver Nanowires as Fillers for Improved Thermal Conductivity, *Mater. Res. Express*, 2017, **4**(1), 015018, DOI: 10.1088/2053-1591/aa55b3.

63 Y. Yin, Y. Lu, Y. Sun and Y. Xia, Silver Nanowires Can Be Directly Coated with Amorphous Silica To Generate Well-Controlled Coaxial Nanocables of Silver/Silica, *Nano Lett.*, 2002, **2**(4), 427–430, DOI: 10.1021/nl025508+.

64 P. Lu, Z. Qu, Q. Wang, Y. Yuan, E. Cheng and M. Zhao, Electrical-Field Induced Nonlinear Conductive Characteristics of Polymer Composites Containing SiO_2-Decorated Silver Nanowire Hybrids, *J. Inorg. Organomet. Polym. Mater.*, 2019, **29**(6), 2116–2123, DOI: 10.1007/s10904-019-01170-8.